Title

Genome-Wide Screening Reveals CSDE1 as a Novel Regulator of the LDL Receptor

Authors

Geoffrey A. Smith, MD PhD[1,2]; Akhil Pampana, MS[3,4]; Pradeep Natarajan, MD[3,4,5]; Kevan M. Shokat, PhD[1,6]; John S. Chorba, MD[7]*

Affiliations

[1]Department of Cellular and Molecular Pharmacology, University of California San Francisco
[2]Present Affiliation: Boston Children's Hospital, Boston MA
[3]Cardiovascular Research Center, Massachusetts General Hospital, Boston MA
[4]Program in Medical and Population Genetics, Broad Institute of Harvard and MIT, Cambridge MA
[5]Department of Medicine, Harvard Medical School, Boston MA
[6]Howard Hughes Medical Institute, University of California San Francisco
[7]Division of Cardiology, Zuckerberg San Francisco General and Department of Medicine, University of California San Francisco
*Correspondence to: john.chorba@ucsf.edu

Abstract

In humans, clearance of LDL cholesterol, which causes atherosclerotic heart disease, is mediated by the hepatic LDL receptor (LDLR)[1]. As a result, therapies that upregulate the LDLR are highly effective treatments for atherosclerosis[2]. Since cardiovascular disease remains the leading cause of death in Western countries[3], we sought to identify regulators of the LDLR beyond the known genetic causes of familial hypercholesterolemia. Here we show that CSDE1, an RNA-binding protein involved in mRNA stability[4], enhances LDLR mRNA degradation to modulate LDLR expression and function. Using parallel phenotypic genome-wide screens, based on the CRISPR interference platform[5], we identified over 100 specific regulators of surface LDLR expression in HepG2 cells, characterized their effects on LDLR function, and leveraged pharmacologic strategies to probe their mechanistic pathways. Among our hits, we found that CSDE1 participates in post-translational control of the LDLR independent from well-established, and clinically exploited, transcriptional and lysosomal regulatory mechanisms. Overall, our results reveal a network of novel LDLR modulators left undiscovered by human genetics, many of which have phenotypic strengths similar to *bona fide* targets in the clinic, offering hope for new therapeutic strategies against atherosclerosis. We anticipate that our approach of modelling a clinically relevant phenotype in an *in vitro* experimental system amenable to a forward genetic screen, followed by high throughput validation and mechanistic pharmacologic dissection, will serve as a template for the identification of novel therapeutic targets for other disease states.

Graphical Abstract

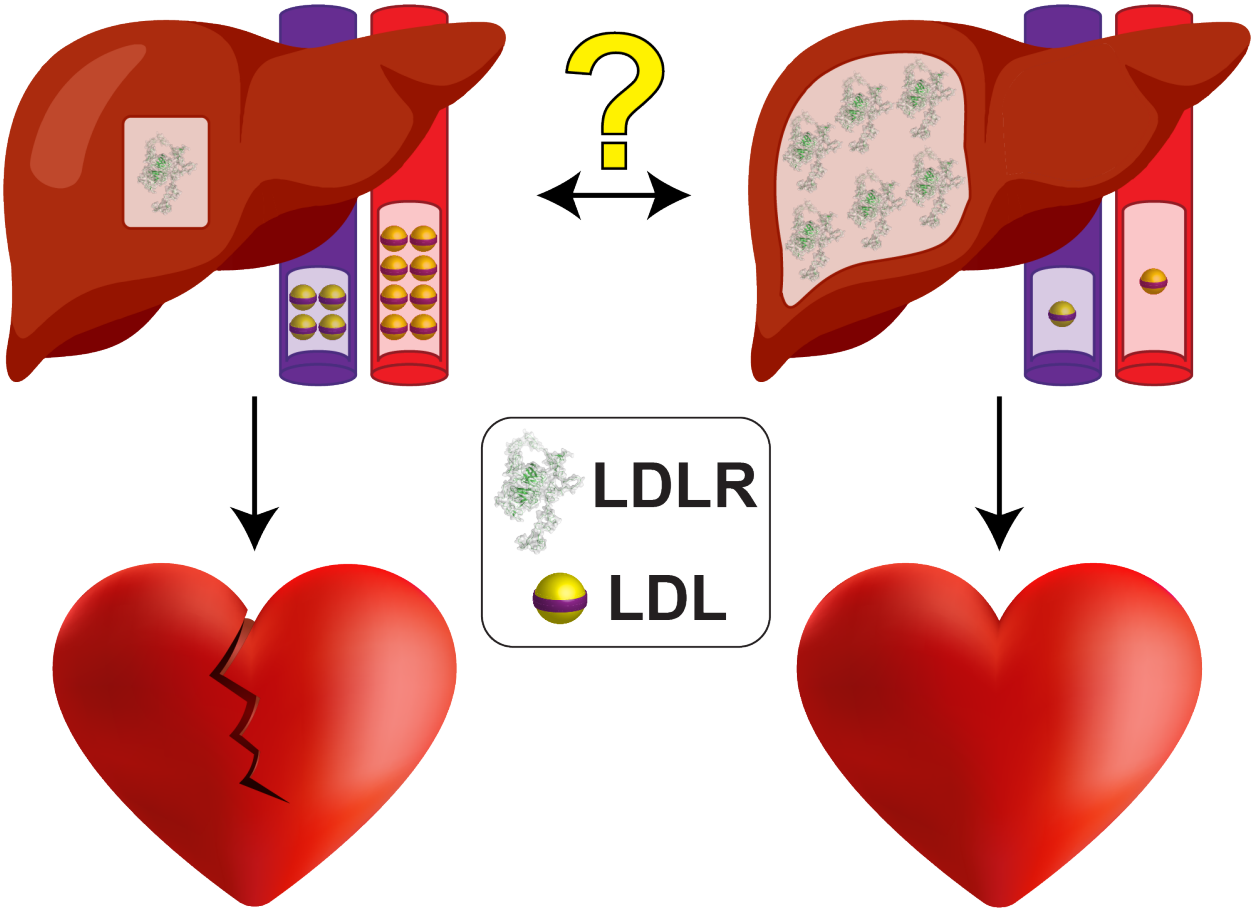

Introduction

Atherosclerosis leads directly to cardiovascular disease and stroke, the leading causes of death in the United States[3]. The causal relationship between atherosclerosis and circulating low density lipoprotein (LDL) is well established[6]. Because the LDL receptor (LDLR) in the liver clears LDL from the bloodstream, therapies that upregulate hepatic LDLR function lower LDL, and by extension, reduce cardiovascular events[2]. Moreover, lowering LDL below the levels achievable by HMG-CoA reductase inhibitors (statins) improves clinical outcomes without adverse effects[7,8]. Though there is a theoretical level at which LDL could get too low, large clinical trials have yet to show the lower bound where cardiovascular protection ends or adverse outcomes occur[9,10]. Accordingly, there is strong clinical interest in other therapeutic strategies to further lower LDL.

The genetics of familial hypercholesterolemia (FH), which manifests with an isolated elevation in serum LDL, underlies the clinical success of two highly effective anti-atherosclerotic therapies: statins and PCSK9 inhibitors. Yet estimates suggest that 20-40% of Mendelian FH remains unexplained outside of the four major causes: *LDLR*, *APOB*, *PCSK9*, and *LDLRAP1*[11,12]. This implies that additional regulators of LDLR function exist. In conjunction with an appropriate experimental model, advances in forward genetics can now enable searches for disease-specific effects across the entire genome, which cannot be completely covered by sporadic natural variants in observational studies.

We therefore employed a genome-wide CRISPR interference (CRISPRi) screen to identify genetic factors involved in LDLR regulation, using cell-surface expression of the LDLR as our readout. We cross-referenced our results with large-scale genomic data to support relevance *in vivo* and prioritize hits. To validate our findings, we used a functional assay of LDL uptake to mimic the clinically relevant effect *in vitro*[13]. We leveraged pharmacology to perturb known pathways of LDLR regulation, providing insights into the mechanistic roles of our hits and the potential for synergy with current therapies. Finally, we show that CSDE1, a top-performing hit, acts independently from current therapeutic targets by promoting the degradation of the LDLR mRNA. Overall, our results reveal novel factors modulating LDLR function with similar strength to current therapeutic targets, provide a framework to select promising new targets against atherosclerosis, and illustrate a generalizable approach to identify new therapeutic strategies in human disease states.

Results

A Genome-Wide CRISPR Interference Screen for LDL Receptor Regulation

We engineered the HepG2 cell line, which models the regulation of the LDLR[14], to constitutively express an inactive Cas9 fused to the KRAB repressor, enabling the knockdown of any given gene with an appropriate sgRNA (Fig. 1A)[5,15,16]. Because mutations in *LDLR* are the primary Mendelian cause of FH, and both statins[17,18] and PCSK9 inhibitors[19–21] increase cell surface LDLR, we chose surface LDLR staining for our selection. To focus on factors which preferentially affect the LDLR over other receptors, we performed a parallel screen for regulators of the transferrin receptor (TFR). This critical player in iron metabolism shares a clathrin-mediated intake mechanism, but is otherwise orthogonally regulated from the LDLR[22,23]. Prior to our screen, we confirmed both dCas9-KRAB activity and an appropriate dynamic range for both LDLR and TFR regulation by transduction of the cells with sgRNAs expected to regulate the receptors in either direction (Extended Data Fig. 1)[24,25].

We next performed our pooled screens in parallel by transducing a library encoding sgRNAs with 5-fold coverage of the entire human genome[5]. We then selected the cells at the upper and lower third of receptor expression by FACS and quantified the sgRNAs for each population via

deep sequencing (Extended Data Fig. 2, Supplemental Tables 1-4). We compared the degree of enrichment in the high expressing to the low expressing cells (defined as ρ, Fig. 1b). We also compared the high and low receptor expressing cells to the unsorted population (defined as τ or γ, respectively) and included these results in our final hit count. This resulted in 130 total hits for the LDLR and 186 hits for the TFR (Extended Data Table 1). We hypothesized that hits with shared phenotypes would likely have global effects on surface receptors, leaving us with 117 hits specific for LDLR regulation (Fig. 1c, Extended Data Table 1). Gene ontology (GO) analysis[26] revealed a 15-fold enrichment for cholesterol metabolism as a biologic process (11 total hits, $p = 5.7 \times 10^{-10}$), providing confidence that we recapitulated our target biology. The hits also included 48 members of potentially druggable protein classes, and 22 hits were unclassified in GO databases (Extended Data Table 3).

Cross-referencing Human Genetic Datasets Identifies LDLR Regulators in vivo

We next curated genes associated with serum LDL cholesterol (LDL-C) from published genome-wide association studies (GWAS)[27–29], comparing them to our list of hits. Intriguingly, only 13 of these genes overlapped with our results (Fig. 1d), even when we relaxed our threshold for hit selection. Since the modest overlap may reflect the stringent statistical cutoffs required for multiple hypothesis testing across the entire genome, we turned to 390,375 UK Biobank participants with genome-wide genotypes and known plasma lipids (Extended Data Table 2) to search for variants associated with LDL-C amongst only our hits[30]. We filtered to nonsynonymous protein coding variants in these hits by a threshold minor allele frequency (>0.001) and minimum statistical significance (Extended Data Table 3). Here, we found an association between increased LDL-C and a premature stop codon in *BCAM*. We also observed missense variants in *BCAM* associating with either higher or lower LDL-C, suggesting that this pathway may be tunable. Additionally, we also found missense variants in *MSMO1*, *C6orf132*, and *HNF4A*, and a splice variant in *TIMELESS*, associated with elevated LDL-C. This suggests that these hits, at least, are functional in the human and merit further evaluation. The results also suggest that the accessible "genomic space" of the CRISPRi and GWAS strategies is only partially overlapping.

Regulators of Surface LDL Receptor Expression Affect Functional Uptake of LDL

To validate our screen results, we generated CRISPRi HepG2 cells harboring either of the two top-scoring sgRNAs for 77 of our hits as well as established controls. We preferentially tested hits with an increase in surface LDLR upon inhibition, as well as those with potentially druggable functions or lacking associated GO terms. Since surface receptor expression might not necessarily correlate to increased function, we evaluated both LDLR and TFR surface phenotypes alongside a functional assay of LDL uptake. Lastly, as knockdowns could also cause growth phenotypes, we assayed the number of cells surviving to FACS analysis as a rough proxy for viability.

We recapitulated the phenotypes for receptor expression for at least one of the guides in the majority of the hits (55 genes, 71% of those tested, Supplemental Table 5). Moreover, for 40 of these genes, both sgRNAs independently validated, suggesting against an off-target effect. We visualized these hits based on their effects, at the single cell level, on LDLR and TFR expression, the LDLR/TFR ratio, functional LDL uptake and number of cells surviving to analysis (Fig. 2). Notably, most knockdowns had functional effects on LDL uptake of similar or greater magnitude than our *HMGCR* or *PCSK9* controls, the *bona fide* targets in the clinic. Knockdown of genes involved in cell proliferation and cytokinesis (*EIF3D*[31], *PRIM1*[32], *POLD2*[33], *TIMELESS*[34], *SON*[35], and *CIT*[36]) had fewer number of cells survive to flow cytometry. This

survival information can help deprioritize potential targets with what will likely be too narrow a therapeutic window.

Knockdown of hits expected to alter cellular cholesterol balance or transcriptionally regulate the LDLR showed congruent directional effects between LDLR expression and function (Fig. 2). For genes in the enzymatic pathway of cholesterol metabolism[37] (*HMGCS1* and *MSMO1*), this is consistent with activation of SREBP2 mediated LDLR transcription. For transcription factors (*HNF1A*[38], *HNF4A*[39], *ONECUT1*[40], and *ZEB1*[41]), this is consistent with an effect on LDLR transcription itself. HNF1A, for one, is known to promote the transcription of PCSK9[42], and therefore a reduction in PCSK9-mediated LDLR degradation could explain the particularly impressive phenotype of the *HNF1A* knockdown. Knockdowns of *SLC25A27*, a mitochondrial uncoupling protein[43], and *ABCA4*, a known lipid transporter[44], both exhibited reductions in LDLR expression and function (Fig. 2). These genes could plausibly induce a negative lipid balance, which could increase LDL uptake via both LDLR dependent and independent mechanisms.

Targeting of hits that either affect multiple transcriptional pathways or regulate endocytosis showed discordance between LDLR expression and function. Knockdown of *TRIB1*, a GWAS hit[27] encoding a pseudokinase that regulates the COP1 E3 ligase[45,46] and affects multiple transcription factors[47], showed this phenotype. In the mouse, TRIB1 overexpression lowers serum cholesterol, while the knockout has the opposite effect[48,49], consistent with our results. Knockdown of *AP2M1*, a TFR screen hit that encodes an adaptor protein required for endocytosis[50], was similar, consistent with an accumulation of non-functional receptors at the cell surface. This same phenotype, though specific to the LDLR, was seen with knockdown of *BCAM*, a membrane cell adhesion molecule[51] identified by GWAS[29], and *TMEM217*, an uncharacterized transmembrane protein (Figs. 2 and Extended Data Fig. 4). This suggests that these proteins could have a similar endocytosis adaptor function specific for the LDLR, akin to *LDLRAP1*[52], in which mutations cause a recessive form of FH.

Pharmacologic Inhibition of Clinically Relevant Pathways Provides Mechanistic Insight into Putative LDLR Regulators

We then turned to pharmacology to perturb specific pathways of LDLR regulation. We hypothesized that hits might alter cholesterol metabolism, LDLR recycling, or a yet unspecified pathway. By combining CRISPRi knockdown with either a statin, to inhibit endogenous cholesterol biosynthesis[53,54], or a PCSK9 inhibitor, to arrest LDLR lysosomal degradation[21], and assessing the combined effect, we inferred mechanistic information about the target gene. Antagonism would suggest perturbation within the same pathway, while simple additivity would suggest an independent mechanism. Furthermore, we hypothesized that additive or synergistic effects between a clinically validated therapy and a hit gene would triage promising therapeutic targets.

We therefore evaluated the receptor expression and function phenotypes for 29 of our hits in the presence or absence of a statin[55] or PF-846, a selective inhibitor of PCSK9 translation[56,57] (Fig. 3, Supplemental Table 6). As expected, both statin and PF-846 treatment increased LDLR expression and function (Fig. 3, legends). We calculated a synergy score, defined as the $\log_2$ fold change of the relative effect of CRISPRi knockdown in the presence of compound over that with the DMSO vehicle. A positive value indicated synergy, and a negative value indicated antagonism.

Upon knockdown, regulators of cholesterol biosynthesis (*SREBF2*, *HMGCS1*, *MSMO1*, and *PMVK*) showed antagonism with the statin, but synergy with PCSK9 inhibition (Fig. 3). This is consistent with the SREBP2 mediated upregulation of PCSK9 transcription that underlies the

clinical synergy between statins and PCSK9 inhibitors. The synergy phenotypes of *MRPL16*, a structural component of the mitochondrial ribosome[58], mirrored these biosynthetic genes (Fig. 3), suggesting that MRPL16 may play a significant role in the mitochondrial generation of metabolic precursors to sterol biogenesis. By contrast, *C6orf132* showed the opposite phenotype: mild synergy with a statin, and mild antagonism with PF-846 (Fig. 3). Given that C6orf132 localizes to the Golgi[59], this suggests it may function by facilitating LDLR delivery to the cell surface, prior to any interaction with extracellular PCSK9. For the transcription factors uncovered in our screen, those with neutral scores with statin therapy (*HNF4A* and *ONECUT1*) are consistent with independent action from SREBP2. Those showing synergy with a statin, and antagonism with PF-846, like *HNF1A*[42] and *ZEB1*, are consistent with a positive effect on PCSK9 transcription.

CSDE1 Regulates the Stability of LDLR mRNA

One of our strongest hits, *CSDE1*, encodes an RNA binding protein that promotes mRNA decay[4]. CSDE1 also binds to the 3' untranslated region (UTR) of LDLR mRNA[60]. As the LDLR 3' UTR consists of AU-rich elements (AREs) implicated in mRNA stability[61], we hypothesized that CSDE1 could mediate the degradation of the LDLR transcript, independent of SREBP2 or PCSK9 mediated mechanisms, thereby explaining its observed expression, function, and synergy phenotypes. To address this, we measured steady-state mRNA levels in the CSDE1 knockdown cells after sterol-depletion. Consistent with our hypothesis, we noted a 2-fold greater mRNA expression of *LDLR* (Fig. 4a), as well as depleted CSDE1 at both the mRNA and protein levels (Fig. 4a, Extended Data Fig. 5), in the CSDE1 knockdowns. To specifically evaluate transcriptional decay, we treated cells with actinomycin D and measured *LDLR* transcript levels over time, normalizing the *LDLR* mRNA levels in both CSDE1 knockdown and negative control cells at T=0. We observed significantly higher *LDLR* mRNA in the CSDE1 knockdowns at all subsequent timepoints (Fig. 4b). The *LDLR* mRNA half-life, modeled by a single-phase decay equation, was nearly 1.5-fold longer for the CSDE1 knockdowns compared to controls ($p=0.013$, Fig. 4b). Notably, *HMGCR* mRNA levels were not significantly different, showing that the effect on mRNA stability was specific to *LDLR* (Fig. 4c).

To probe the relationship of CSDE1 to the LDLR 3' UTR, we transiently expressed a luciferase construct fused to the LDLR 3' UTR in the CSDE1 knockdown cells. We unexpectedly observed decreased luciferase activity in the CSDE1 knockdowns compared to controls (Fig. 4d). This effect was also observed with a luciferase fusion harboring both 5' and 3' UTRs of the LDLR mRNA, but was not seen with either an unmodified luciferase or a luciferase fused to the coding sequence of the LDLR via a P2A sequence[62]. Because all constructs produced essentially the same luciferase protein, the difference in luciferase activity was mediated by the identity of the mRNA itself. Taken together, we conclude that CSDE1 mediates decay of the LDLR mRNA and interacts with the LDLR 3' UTR, but this interaction is not sufficient for decay. Instead, our data suggest that CSDE1 requires other factors to mediate decay, and without them, a CSDE1-3' UTR interaction can paradoxically increase the expression of a transcript, at least in a heterologous expression system.

Discussion

The powerful biology of the LDLR is unquestioned in cardiovascular medicine[63]. Since their introduction, statins, which upregulate the LDLR, have become a major public health success, and with the discovery of PCSK9, and the therapeutic antibodies targeting it, patients can reach much lower LDL levels than is achievable by statins alone, with minimal toxicity[9]. Together, this suggests that we can push further on this LDL-LDLR axis and still get a clinical benefit.

In this study, we modelled the clinically relevant phenotype of LDLR expression and function in an experimental system amenable to emerging genome-wide CRISPR screening technologies. To generalize our findings, we turned to large-scale genomics grounded in clinical phenotypes. To infer mechanistic data otherwise absent from a large-scale screen, we combined validation with pharmacologic perturbation to identify regulators acting within clinically targeted pathways. When synthesized together, we produce an exploratory map of potential regulatory mechanisms for the LDLR (Extended Data Fig. 6), which represent not just promising targets but also pathways likely to be impacted by therapies already in use in the clinic. Beyond the LDLR, we anticipate that the combination of these orthogonal methods will serve as a useful template for discovering promising new targets in other diseases.

We have shown that *CSDE1*, one of our strongest hits, regulates LDLR levels in HepG2 cells by promoting decay of the *LDLR* mRNA transcript. This data lies in concert with CSDE1's destabilizing effects on other transcripts, such as c-Fos[4]. However, as an RNA chaperone, CSDE1 can have a variety of effects, from mRNA stabilization[64] to promotion or inhibition of translation[65–68], dependent on the identity of the RNA it binds and the cofactors with which it interacts. The unexpected increase in transcript expression mediated by the 3' UTR in the CSDE1 knockdown cell line suggests other factors are at play, and without them, CSDE1 could mediate an opposite function. In this vein, it is notable that both poly(A)-binding protein and hnRNP D, which also play roles in RNA decay, each associate with the *cis*-acting elements on c-Fos[4,69] and LDLR[60,70] responsible for rapid transcript turnover. The mechanistic relationship between CSDE1 and the 3' UTR, any additional *cis*-acting elements, and other cofactors remains outstanding, and future studies are warranted to assess whether our findings extend outside of our heterologous expression system.

Irrespective of the mechanism, prolonging LDLR stability *in vivo* by deletion of these 3' UTR regions results in less atherogenic serum lipid profiles[71], illustrating its promise as a strategy to lower LDL and protect against atherosclerosis. Indeed, several small molecules, including triciribine[72] and berberine[70,73], have stabilizing effects on LDLR mRNA. From the standpoint of target validation, whether CSDE1 inhibition affects other transcripts, or other tissues[7475], remains an important question. In Huh7 liver cells, siRNA knockdown of CSDE1 promotes apoptosis[76], which we did not observe in our HepG2 based study. Though enthusiasm for CSDE1 as a potential target should be restrained pending *in vivo* validation in a mammalian system, advances in liver-specific targeting of gene silencing agents[77] and small molecules[78] could potentially overcome these off-target concerns, particularly in other tissues.

Acknowledgements
We thank Max Horlbeck for guidance with the CRISPRi system. We also thank Bryan Lau, Brian Black, and Roland Wu for technical assistance and helpful discussion. Plasmids for the CRISPRi system were a generous gift from Luke Gilbert and Jonathan Weissman. We thank the Gladstone Institutes Flow Cytometry core facility for their assistance with flow cytometry experiments. UK Biobank analyses were conducted using the UK Biobank resource under application 7089.

Author Contributions
Study design: J.S.C. Execution of screen and data processing: G.A.S. Validation experiments: J.S.C. Genomic analysis: A.P., P.N. Data analysis: G.A.S., P.N., K.M.S., J.S.C. Preparation of manuscript: J.S.C. Review and revision of manuscript: G.A.S., P.N., K.M.S., J.S.C.

Funding Sources
P.N. is supported by a Hassenfeld Scholar Award from the Massachusetts General Hospital, the NIH/NHLBI (R01 HL-142711, R01 HL-148565, and R01 HL-148050), and the Fondation Leducq (TNE-18CVD04). K.M.S. is supported by the Howard Hughes Medical Institute. J.S.C. is supported by the NIH/NHLBI (K08 HL-124068 and R03 HL-145259), a Pfizer ASPIRE Cardiovascular Award and the Harris Fund and Research Evaluation and Allocation Committee of the UCSF School of Medicine.

Competing Interests
P.N. reports investigator-initiate grant support from Amgen, Apple, and Boston Scientific, and personal fees from Apple, Blackstone Life Sciences, and Novartis, all unrelated to the present work. K.M.S. has consulting agreements for the following companies involving cash and/or stock compensation: Black Diamond Therapeutics, BridGene Biosciences, Denali Therapeutics, Dice Molecules, eFFECTOR Therapeutics, Erasca, Genentech/Roche, Janssen Pharmaceuticals, Kumquat Biosciences, Kura Oncology, Merck, Mitokinin, Petra Pharma, Revolution Medicines, Type6 Therapeutics, Venthera, Wellspring Biosciences (Araxes Pharma). J.S.C. has received consulting fees from Gilde Healthcare and is an unpaid scientific advisor to Eko, both unrelated to this work.

Data Availability Statement
Additional supporting data are available upon request from the corresponding author. All requests for raw and analyzed data, and materials, including plasmids or cell lines, generated in this study will be responded to promptly. UK Biobank data is available by application to the UK Biobank.

Methods
Plasmids and Cloning
SFFV-dCas9-BFP-KRAB (Addgene 46911), CRISPRi/a v2 (Addgene 84832), pMD2.G, dR8.91, and the hCRISPRi v2 top5 sgRNA library (Addgene 83969) were gifts from L. Gilbert and J. Weissman. Oligonucleotides of the protospacers of validated sgRNA sequences[5], as well as those for PCR amplification and isothermal assembly, were obtained from Elim Biopharmaceuticals (Hayward CA). Protospacers were cloned into the CRISPRi/a v2 vector using restriction enzyme digest (BlpI and BstXI, ThermoFisher, Waltham MA) and ligation with 10× T4 ligase (NEB, Ipswich MA). pLuc2 and was created by PCR expansion of the target luciferase from pGL4Luc-RLuc (Addgene 64034) and isothermal assembly[79] into the pcDNA5/FRT/TO backbone (ThermoFisher). pSS-NLuc was created by PCR expansion of the target luciferase from pNL1.1 (Promega, Madison WI) into a vector containing the PCSK9 signal sequence from the same backbone[80]. pLuc2-P2A-LDLR was created by PCR expansion of the

coding region of LDLR (HsCD00004643, DNASU, Tempe AZ) and isothermal assembly into pLuc2, using custom oligonucleotides to add the P2A linker. pLuc2-3'UTR was created by PCR amplification of custom gene synthesis of the entire 3' UTR of LDLR mRNA (NCBI Reference Sequence NM_001252658.1,Twist Biosciences, South San Francisco CA) and isothermal assembly into pLuc2. pLuc2-5'3'UTR was created by isothermal assembly into pLuc2-3'UTR, using custom oligonucleotides to add the 5' UTR (NCBI Reference Sequence NM_001252658.1). All plasmids were confirmed by Sanger sequencing. Expansion of the top5 sgRNA library was as previously described[15].

Cell Culture and Lentiviral Production

HepG2 (ATCC HB-8065) and derivatives were cultured in low-glucose DMEM (1 g/L, ThermoFisher) with 10% FBS (Axenia BioLogix, Dixon CA), GlutaMax (ThermoFisher) and 1× penicillin-streptomycin (ThermoFisher), and sent thrice through a 21g needle during passaging to minimize cell clumping. HEK-293T (ATCC CRL-3216) were cultured in standard DMEM (ThermoFisher) with 10% FBS. All cell lines were cultured at 37 °C at 5% CO_2, seeded for approximately 50% confluency at the time of experiment, and were confirmed free of *Mycoplasma* contamination by the MycoAlert PLUS Mycoplasma Detection Kit (Lonza, Switzerland). Lentivirus was produced in 293T cells by transfection of dR8.91, pMD2.G, and the appropriate pLKO-derived vector (at ratios of 8 µg, 1 µg, and 8 µg, respectively, per 15 cm dish) with Trans-LT1 (Mirus Bio, Madison WI), according to the manufacturer's instructions. Viral harvest media was supplemented with Viralboost (Alstem, Richmond CA), collected 2-3 days after transfection, and filtered through 0.44 µm polyvinylidene difluoride filters and either frozen for storage at -80 °C or used immediately for transduction.

Generation of CRISPRi Cell Lines

All cell lines were transduced using virus-containing supernatant in the presence of 8 µg/ml polybrene (Millipore-Sigma, St. Louis MO). HepG2 expressing dCas9-KRAB were derived by transduction with lentivirus harboring SFFV-dCas9-BFP-KRAB, followed by two rounds of FACS for BFP-positive cells on a BD FACSAria II. dCas9-KRAB HepG2 with individual targeting sgRNAs were derived by transduction with lentivirus harboring the desired sgRNA, followed by 48 hrs of puromycin selection (2 mg/ml, InvivoGen, San Diego CA), prior to experiments.

Quantitative Real-Time PCR

dCas9-KRAB HepG2 stably expressing an appropriate sgRNA were harvested, lysed, and total RNA was extracted via the RNeasy Mini Kit (Qiagen, Germantown MD). RNA was converted into cDNA using qScript cDNA SuperMix (QuantaBio, Beverly MA) following the manufacturer's instructions. RT-qPCR was performed against indicated targets with PrimeTime qPCR primers (IDT, Coralville IA) using the SYBR Select Master Mix (ThermoFisher) according to the manufacturer's instructions on a CFX96 Touch Real-Time PCR Detection System (BioRad, Hercules CA). Fold changes were calculated using ΔΔCt analysis, normalizing each sample to *B2M* controls, using CFX Maestro software (BioRad).

Receptor Expression Analysis

1-2 days prior to analysis, dCas9-HepG2 cells and derivatives were cultured in low-glucose DMEM with 5% lipoprotein deficient serum (Kalen Biomedical, Germantown MD). Prior to analysis, cells were dissociated with Accutase (Innovative Cell Technologies, San Diego CA), collected, washed in PBS (ThermoFisher), live-dead stained with Ghost Dye Red 780 (1:1000 dilution, Tonbo Biosciences, San Diego CA), washed, and then stained with the indicated antibody in FACS buffer (PBS with 1% FBS, 10 U/ml DNAse I, GoldBio, St. Louis MO) for 30 minutes on ice with gentle agitation. Cells were washed, resuspended in FACS buffer, filtered to give a single cell suspension, and placed on ice. Cells were then analyzed on either a BD

Fortessa, BD LSRII or BD FACSAria II, or sorted on a BD FACSAria II, depending on the experiment. In general, gating excluded cells positive for live-dead staining and included only the cells positive for the level of BFP expression induced by the CRISPRi/a v2 vector. FACS analysis and figure preparation was performed with FlowJo v10 (BD, Ashland OR).

Genome-Wide CRISPRi Screen

The screen was conducted similarly to prior descriptions[5,15,81]. Approximately 200 x 10^6 dCas9-KRAB HepG2 were transduced with hCRISPRi-v2 top 5 sgRNAs/gene lentivirus at an MOI of ~0.5 , and with polybrene at 8 mg/ml, on day 1. Cells were grown on 15-cm dishes, subdivided into four replicates immediately upon transduction (biological duplicate for each screen), and reseeded every 3-4 days as necessary to avoid overconfluence. Cells were selected with puromycin (2 mg/ml) from day 2 through day 6. On day 5, cells for the LDLR sort were placed in DMEM with lipoprotein depleted serum (5%). On day 7, approximately 50 x 10^6 cells from 2 replicates were live-dead stained and stained for LDLR as described above, and then two-way sorted on a BD FACSAria II for the top and bottom 33% by LDLR expression. Cells were spun down, washed in PBS and frozen at -80 ºC. On day 8, the sort was repeated except in one replicate, cells were stained for TFR instead of LDLR and then sorted as per above. Genomic DNA was isolated using a NucleoSpin Blood DNA extraction kit (Macherey-Nagel, Bethlehem PA). The sgRNA-containing region was PCR-amplified with NEBNext Ultra II Q5 MasterMix (NEB), acrylamide gel-purified, and size-selected by SPRI beads (Beckman Coulter, Indianapolis IN), all as previously described, prior to sequencing on an Illumina HiSeq 4000.

Screen Processing

Sequencing data were aligned to the top5 library, counted, and quantified using the ScreenProcessing pipeline (accessed from https://github.com/mhorlbeck/ScreenProcessing[5] 4/25/2019). Phenotypes and Mann-Whitney *P* values were determined as previously described[5], with the phenotypes defined as follows: ρ indicated the comparison in high-expressing vs. low expressing cells, τ indicated the comparison in high-expressing vs. unsorted cells, and γ indicated the comparison in low-expressing vs. unsorted cells. Counts from 4 guides were removed from the final analysis as there was evidence of contamination from individually cloned plasmids (PCSK9_+_55505255.23-P1P2, HMGCR_+_74633053.23-P1P2, TFRC_-_195808987.23-P1P2, ACO1_-_32384733.23-P1P2). A hit threshold of 7 (normalized phenotype z score $\times$ -log10(p-value) $\geq$ 7)[15] was used to identify hits from ρ, τ, and γ phenotypes, which were then compiled. Identical analysis of the TFR screen was used to prioritize hits unique to LDLR regulation. Gene ontology analysis was performed using the PANTHER Classification System database (v15)[26,82]. For relaxation of the hit threshold for comparison to GWAS studies, a score of 6 was used. Cellular localization of hits was imputed by manual curation from UniProt[83] and the Human Protein Atlas[59].

Human Genomic Analysis

Protein coding variants for hits validated at the individual sgRNA level were assayed in the UK Biobank[84] for associations with LDL-C. In the setting of a statin medication, LDL-C was divided by 0.7 as before[28]. Genotyping and imputation was performed in the UK Biobank as previously described[30], and nonsynonymous protein coding variants with minor allele frequencies greater than 0.001 were considered. Efficient linear mixed models adjusting for age, sex, genotyping array, and principal components of ancestry were employed, using BOLT-LMM[85]. Statistical significance was assigned at α = 0.05/117 = 0.000427 to account for multiple hypothesis testing.

Validation Experiments of Individual sgRNAs

Cloning of protospacers, as described above, was performed in 96-well plate format until selecting individual colonies. Lentiviral production in 293T, transduction of dCas9-KRAB HepG2 with lentiviral sgRNA vectors, and receptor expression and LDL uptake assays were similarly performed in 96-well plate format to maximize throughput.

LDL Uptake Assays

Assays were performed as previously described[13] with the following modifications. dCas9-HepG2 cells harboring individual sgRNAs were treated similarly to receptor expression analysis, except that prior to harvest, cells were washed and then treated with 5 µg/ml 1,1'-dioctadecyl-3,3,3',3'-tetramethylindocarbocyanine perchlorate (DiI) labeled LDL (Kalen Biomedical) in low-glucose DMEM with 0.5% BSA (MilliporeSigma) for 1 hr at 37 °C. Cells were then washed, collected, and prepared for FACS analysis, as described above, but without antibody labelling.

Pharmacologic Synergy Experiments

Receptor and LDL uptake assays were performed as described, with cells treated overnight with either simvastatin (6 µM, MilliporeSigma), PF-6846 (10 µM, MilliporeSigma), or DMSO vehicle (final concentration of 0.5%) overnight prior to analysis.

mRNA Decay Experiments

Engineered dCas9-HepG2 cell lines harboring sgRNAs against CSDE1 (CSDE1_+_115300577.23-P1P2) and a negative control (Unassigned=negZNF335_-_44601297.24-all) were seeded into 12 well plates at 5e5 cells per well in HepG2 growth medium. After 24 hrs, cells were washed and changed into sterol-depleting media (low-glucose DMEM with 5% lipoprotein-deficient serum) supplmeneted with 6 µM simvastatin. After an additional 24 hrs, actinomycin D (MilliporeSigma) was added at 5 µg/ml, and cells were harvested as described at the indicated timepoints.

Immunoblots

Engineered dCas9-HepG2 cell lines harboring appropriate sgRNAs were grown in growth medium and harvested with 0.25% trypsin digestion. Cells were washed and lysed in lysis buffer on ice (50 mM Tris-HCl pH 7.4, 150 mM NaCl, 0.1% NP-40). Lysates were clarified at 21,000 × *g* for 10 min, and the supernatant was recovered. Equivalent amounts of lysates were resolved on 4-12% Bis-Tris NuPAGE gels (ThermoFisher), transferred to nitrocellulose, probed with primary and secondary antibodies as noted (see Table) in 5% BSA in TBS-T, and visualized on an Odyssey imaging system (LI-COR, Lincoln NE).

Dual-Luciferase Assays

Engineered dCas9-HepG2 cells were seeded into opaque white 96 well plates, at 2.2×10^4 cells per well, in 100 µL growth medium the day prior to transfection. On day of transfection, 100 ng of orthogonal luciferase constructs (Luc2 and secreted NLuc) in 10 µL OptiMEM (ThermoFisher) were transfected at a 9:1 w/w ratio, with 6 replicates per construct, using Lipofectamine 3000 (ThermoFisher) according to the manufacturer's instructions. After 48 hours at 37°C and 5% CO_2, 20 µL of medium was removed from each plate and aliquoted into a separate 96 well plate. Firefly luciferase activity was evaluated in the plates containing the cells by adding 80 µL of a 2× firefly lytic assay buffer (100 mM Tris-HCl pH 7.7, 50 mM NaCl, 2 mM $MgCl_2$, 0.17% Triton X-100, 10 mM DTT, 0.4 mM coenzyme A, 0.3 mM ATP, and 0.28 mg/ml luciferin (Goldbio))[86]. Nanoluciferase activity was evaluated from the conditioned medium using a non-lytic 2× coelenterazine (Goldbio) reagent as previously described[80]. Raw luminescence was obtained on a Tecan SPARK plate reader (Tecan, San Jose CA) with 1 second integration time.

Readout of firefly luciferase in each well was normalized to the corresponding secreted nanoluciferase control and data was cleaned of outliers (at ROUT = 1%) during analysis.

Statistical Analysis

Fluorescence values from gated populations in flow cytometry experiments were background corrected by unstained controls, and were normalized to the values of the cell line harboring negative control sgRNA. Normalized data were then grouped by the Cochrane method[87], and values for cell lines transduced with individual sgRNAs were compared those of the negative control by T-test with Holm-Sidak correction. For comparison of one-phase decay regression curves in mRNA decay experiments, the extra sum-of-squares F test was used. Pairwise testing to controls was performed in all other experiments using Welch's T-test with Holm-Sidak correction unless otherwise noted. Adjusted p values < 0.05 were considered significant. Statistical analysis was performed using Prism 7 (GraphPad Software, San Diego CA). All experiments were replicated thrice unless otherwise noted.

Table S1 | Reagents

Antibodies				
Target	**Fluorophore**	**Clone**	**Source**	**Dilution / Final Concentration**
Human LDL Receptor	Alexa Fluor 647	472413	R&D Systems	1:100, 2 mg/ml (FACS)
Human Transferrin Receptor	Alexa Fluor 647	29806	R&D Systems	1:100, 2 mg/ml (FACS)
Human Transferrin Receptor	Alexa Fluor 488	29806	R&D Systems	1:100, 2 mg/ml (FACS)
CSDE1	None	62328	Cell Signaling Technology	1:1000 (WB)
beta-Actin	None	8H10D10	Cell Signaling Technology	1:2000 (WB)
Rabbit IgG	IRDye 800CW	926-32211	LI-COR	1:5000, 0.1 µg/ml (WB)
Mouse IgG	IRDye 800CW	926-32210	LI-COR	1:5000, 0.1 µg/ml (WB)
qPCR Primers				
Target	**Reference Sequence**	**Assay ID**	**Source**	**Final Concentration**
B2M	NM_004048(1)	Hs.PT.58v.18759587	IDT	300 nM
LDLR	NM_000527(6)	Hs.PT.58.2004261	IDT	300 nM
HMGCR	NM_000859(2)	Hs.PT.58.41105492	IDT	300 nM
CSDE1	NM_001007553(6)	Hs.PT.58.40309152	IDT	300 nM

References

1. Goldstein JL, Brown MS. The LDL receptor. *Arterioscler Thromb Vasc Biol*. 2009. doi:10.1161/ATVBAHA.108.179564
2. Silverman MG, Ference BA, Im K, et al. Association Between Lowering LDL-C and Cardiovascular Risk Reduction Among Different Therapeutic Interventions. *JAMA*. 2016;316(12):1289. doi:10.1001/jama.2016.13985
3. Xu J, Murphy SL, Kochanek KD, Arias E. *Mortality in the United States, 2018 Key Findings Data from the National Vital Statistics System*.; 2018. https://www.cdc.gov/nchs/data/databriefs/db355_tables-508.pdf#1. Accessed April 22, 2020.
4. Chang TC, Yamashita A, Chen CYA, et al. UNR, a new partner of poly(A)-binding protein, plays a key role in translationally coupled mRNA turnover mediated by the c-fos major coding-region determinant. *Genes Dev*. 2004. doi:10.1101/gad.1219104
5. Horlbeck MA, Gilbert LA, Villalta JE, et al. Compact and highly active next-generation libraries for CRISPR-mediated gene repression and activation. *Elife*. 2016;5. doi:10.7554/eLife.19760
6. Goldstein JL, Brown MS. A Century of Cholesterol and Coronaries: From Plaques to Genes to Statins. *Cell*. 2015;161(1):161-172. doi:10.1016/j.cell.2015.01.036
7. Schwartz GG, Steg PG, Szarek M, et al. Alirocumab and cardiovascular outcomes after acute coronary syndrome. *N Engl J Med*. 2018. doi:10.1056/NEJMoa1801174
8. Sabatine MS, Giugliano RP, Keech AC, et al. Evolocumab and Clinical Outcomes in Patients with Cardiovascular Disease. *N Engl J Med*. 2017;376(18):1713-1722. doi:10.1056/NEJMoa1615664
9. Giugliano RP, Pedersen TR, Park J-G, et al. Clinical efficacy and safety of achieving very low LDL-cholesterol concentrations with the PCSK9 inhibitor evolocumab: a prespecified secondary analysis of the FOURIER trial. *Lancet*. 2017;390(10106):1962-1971. doi:10.1016/S0140-6736(17)32290-0
10. Sabatine MS, Wiviott SD, Im K, Murphy SA, Giugliano RP. Efficacy and safety of further lowering of low-density lipoprotein cholesterol in patients starting with very low levels: A meta-analysis. *JAMA Cardiol*. 2018. doi:10.1001/jamacardio.2018.2258
11. Taylor A, Wang D, Patel K, et al. Mutation detection rate and spectrum in familial hypercholesterolaemia patients in the UK pilot cascade project. *Clin Genet*. 2010;77(6):572-580. doi:10.1111/j.1399-0004.2009.01356.x
12. Garg A, Fazio S, Duell PB, et al. Molecular Characterization of Familial Hypercholesterolemia in a North American Cohort. *J Endocr Soc*. 2019. doi:10.1210/jendso/bvz015
13. Loregger A, Nelson JK, Zelcer N. Assaying Low-Density-Lipoprotein (LDL) Uptake into Cells. In: *Methods in Molecular Biology (Clifton, N.J.)*. Vol 1583. ; 2017:53-63. doi:10.1007/978-1-4939-6875-6_5
14. Knowles BB, Howe CC, Aden DP. Human hepatocellular carcinoma cell lines secrete the major plasma proteins and hepatitis B surface antigen. *Science (80-)*. 1980. doi:10.1126/science.6248960
15. Gilbert LA, Horlbeck MA, Adamson B, et al. Genome-Scale CRISPR-Mediated Control of Gene Repression and Activation. *Cell*. 2014;159(3):647-661. doi:10.1016/j.cell.2014.09.029
16. Mandegar MA, Huebsch N, Frolov EB, et al. CRISPR Interference Efficiently Induces Specific and Reversible Gene Silencing in Human iPSCs. *Cell Stem Cell*. 2016. doi:10.1016/j.stem.2016.01.022
17. Alberts AW, Chen J, Kuron G, et al. Mevinolin: A highly potent competitive inhibitor of hydroxymethylglutaryl-coenzyme A reductase and a cholesterol-lowering agent. *Proc Natl*

Acad Sci U S A. 1980. doi:10.1073/pnas.77.7.3957

18. Brown MS, Faust JR, Goldstein JL, Kaneko I, Endo A. Induction of 3-hydroxy-3-methylglutaryl coenzyme A reductase activity in human fibroblasts incubated with compactin (ML-236B), a competitive inhibitor of the reductase. *J Biol Chem*. 1978.
19. Benjannet S, Rhainds D, Essalmani R, et al. NARC-1/PCSK9 and its natural mutants: zymogen cleavage and effects on the low density lipoprotein (LDL) receptor and LDL cholesterol. *J Biol Chem*. 2004;279(47):48865-48875. doi:10.1074/jbc.M409699200
20. Rashid S, Curtis DE, Garuti R, et al. Decreased plasma cholesterol and hypersensitivity to statins in mice lacking Pcsk9. *Proc Natl Acad Sci U S A*. 2005;102(15):5374-5379. doi:10.1073/pnas.0501652102
21. Chan JC, Piper DE, Cao Q, et al. A proprotein convertase subtilisin/kexin type 9 neutralizing antibody reduces serum cholesterol in mice and nonhuman primates. *Proc Natl Acad Sci U S A*. 2009;106(24):9820-9825. doi:10.1073/pnas.0903849106
22. Aisen P. Transferrin receptor 1. *Int J Biochem Cell Biol*. 2004;36(11):2137-2143. doi:10.1016/j.biocel.2004.02.007
23. Coffey R, Ganz T. Iron homeostasis: An anthropocentric perspective. *J Biol Chem*. 2017;292(31):12727-12734. doi:10.1074/jbc.R117.781823
24. Zelcer N, Hong C, Boyadjian R, Tontonoz P. LXR regulates cholesterol uptake through Idol-dependent ubiquitination of the LDL receptor. *Science*. 2009;325(5936):100-104. doi:10.1126/science.1168974
25. Yoshinaga M, Nakatsuka Y, Vandenbon A, et al. Regnase-1 Maintains Iron Homeostasis via the Degradation of Transferrin Receptor 1 and Prolyl-Hydroxylase-Domain-Containing Protein 3 mRNAs. *Cell Rep*. 2017. doi:10.1016/j.celrep.2017.05.009
26. Mi H, Muruganujan A, Ebert D, Huang X, Thomas PD. PANTHER version 14: more genomes, a new PANTHER GO-slim and improvements in enrichment analysis tools. *Nucleic Acids Res*. 2019;47(D1):D419-D426. doi:10.1093/nar/gky1038
27. Teslovich TM, Musunuru K, Smith A V., et al. Biological, clinical and population relevance of 95 loci for blood lipids. *Nature*. 2010;466(7307):707-713. doi:10.1038/nature09270
28. Natarajan P, Peloso GM, Zekavat SM, et al. Deep-coverage whole genome sequences and blood lipids among 16,324 individuals. *Nat Commun*. 2018;9(1):3391. doi:10.1038/s41467-018-05747-8
29. Liu DJ, Peloso GM, Yu H, et al. Exome-wide association study of plasma lipids in >300,000 individuals. *Nat Genet*. 2017;49(12):1758-1766. doi:10.1038/ng.3977
30. Bycroft C, Freeman C, Petkova D, et al. The UK Biobank resource with deep phenotyping and genomic data. *Nature*. 2018. doi:10.1038/s41586-018-0579-z
31. Lee ASY, Kranzusch PJ, Cate JHD. EIF3 targets cell-proliferation messenger RNAs for translational activation or repression. *Nature*. 2015. doi:10.1038/nature14267
32. Schneider A, Smith RWP, Kautz AR, Weisshart K, Grosse F, Nasheuer HP. Primase activity of human DNA polymerase α-primase. *J Biol Chem*. 1998. doi:10.1074/jbc.273.34.21608
33. Xie B, Mazloum N, Liu L, Rahmeh A, Li H, Lee MYWT. Reconstitution and characterization of the human DNA polymerase delta four-subunit holoenzyme. *Biochemistry*. 2002. doi:10.1021/bi0262707
34. Gotter AL, Suppa C, Emanuel BS. Mammalian TIMELESS and Tipin are Evolutionarily Conserved Replication Fork-associated Factors. *J Mol Biol*. 2007. doi:10.1016/j.jmb.2006.10.097
35. Kim JH, Shinde DNN, Reijnders MRRF, et al. De Novo Mutations in SON Disrupt RNA Splicing of Genes Essential for Brain Development and Metabolism, Causing an Intellectual-Disability Syndrome. *Am J Hum Genet*. 2016. doi:10.1016/j.ajhg.2016.06.029
36. Gruneberg U, Neef R, Li X, et al. KIF14 and citron kinase act together to promote efficient cytokinesis. *J Cell Biol*. 2006. doi:10.1083/jcb.200511061

37. Mazein A, Watterson S, Hsieh WY, Griffiths WJ, Ghazal P. A comprehensive machine-readable view of the mammalian cholesterol biosynthesis pathway. *Biochem Pharmacol*. 2013. doi:10.1016/j.bcp.2013.03.021
38. Rose RB, Bayle JH, Endrizzi JA, Cronk JD, Crabtree GR, Alber T. Structural basis of dimerization, coactivator recognition and MODY3 mutations in HNF-1α. *Nat Struct Biol*. 2000. doi:10.1038/78966
39. Delaforest A, Di Furio F, Jing R, et al. HNF4A regulates the formation of hepatic progenitor cells from human iPSC-derived endoderm by facilitating efficient recruitment of RNA pol II. *Genes (Basel)*. 2019. doi:10.3390/genes10010021
40. Wang K, Holterman AX. Pathophysiologic role of hepatocyte nuclear factor 6. *Cell Signal*. 2012. doi:10.1016/j.cellsig.2011.08.009
41. Wellner U, Schubert J, Burk UC, et al. The EMT-activator ZEB1 promotes tumorigenicity by repressing stemness-inhibiting microRNAs. *Nat Cell Biol*. 2009. doi:10.1038/ncb1998
42. Li H, Dong B, Park SW, Lee H-S, Chen W, Liu J. Hepatocyte nuclear factor 1alpha plays a critical role in PCSK9 gene transcription and regulation by the natural hypocholesterolemic compound berberine. *J Biol Chem*. 2009;284(42):28885-28895. doi:10.1074/jbc.M109.052407
43. Gao CL, Zhu JG, Zhao YP, et al. Mitochondrial dysfunction is induced by the overexpression of UCP4 in 3T3-L1 adipocytes. *Int J Mol Med*. 2010. doi:10.3892/ijmm_00000315
44. Quazi F, Molday RS. Differential phospholipid substrates and directional transport by ATP-binding cassette proteins ABCA1, ABCA7, and ABCA4 and disease-causing mutants. *J Biol Chem*. 2013. doi:10.1074/jbc.M113.508812
45. Kung JE, Jura N. The pseudokinase TRIB 1 toggles an intramolecular switch to regulate COP 1 nuclear export . *EMBO J*. 2019. doi:10.15252/embj.201899708
46. Murphy JM, Nakatani Y, Jamieson SA, Dai W, Lucet IS, Mace PD. Molecular Mechanism of CCAAT-Enhancer Binding Protein Recruitment by the TRIB1 Pseudokinase. *Structure*. 2015. doi:10.1016/j.str.2015.08.017
47. Soubeyrand S, Martinuk A, McPherson R. TRIB1 is a positive regulator of hepatocyte nuclear factor 4-Alpha. *Sci Rep*. 2017. doi:10.1038/s41598-017-05768-1
48. Bauer RC, Sasaki M, Cohen DM, et al. Tribbles-1 regulates hepatic lipogenesis through posttranscriptional regulation of C/EBPα. *J Clin Invest*. 2015. doi:10.1172/JCI77095
49. Burkhardt R, Toh SA, Lagor WR, et al. Trib1 is a lipid- and myocardial infarction-associated gene that regulates hepatic lipogenesis and VLDL production in mice. *J Clin Invest*. 2010;120(12):4410-4414. doi:10.1172/JCI44213; 10.1172/JCI44213
50. Motley A, Bright NA, Seaman MNJ, Robinson MS. Clathrin-mediated endocytosis in AP-2-depleted cells. *J Cell Biol*. 2003. doi:10.1083/jcb.200305145
51. Parsons SF, Mallinson G, Holmes CH, et al. The Lutheran blood group glycoprotein, another member of the immunoglobulin superfamily, is widely expressed in human tissues and is developmentally regulated in human liver. *Proc Natl Acad Sci U S A*. 1995. doi:10.1073/pnas.92.12.5496
52. Mishra SK, Keyel PA, Edeling MA, Dupin AL, Owen DJ, Traub LM. Functional dissection of an AP-2 β2 appendage-binding sequence within the autosomal recessive hypercholesterolemia protein. *J Biol Chem*. 2005. doi:10.1074/jbc.M501029200
53. Radhakrishnan A, Goldstein JL, McDonald JG, Brown MS. Switch-like Control of SREBP-2 Transport Triggered by Small Changes in ER Cholesterol: A Delicate Balance. *Cell Metab*. 2008. doi:10.1016/j.cmet.2008.10.008
54. Horton JD, Shah NA, Warrington JA, et al. Combined analysis of oligonucleotide microarray data from transgenic and knockout mice identifies direct SREBP target genes. *Proc Natl Acad Sci U S A*. 2003;100(21):12027-12032. doi:10.1073/pnas.1534923100
55. Scandinavian Simvastatin Survival Study Group. Randomised trial of cholesterol lowering

in 4444 patients with coronary heart disease: the Scandinavian Simvastatin Survival Study (4S). *Lancet*. 1994. doi:10.1016/S0140-6736(94)90566-5

56. Lintner NG, McClure KF, Petersen D, et al. Selective stalling of human translation through small-molecule engagement of the ribosome nascent chain. Khosla C, ed. *PLoS Biol*. 2017;15(3):e2001882. doi:10.1371/journal.pbio.2001882
57. Li W, Ward FR, McClure KF, et al. Structural basis for selective stalling of human ribosome nascent chain complexes by a drug-like molecule. *Nat Struct Mol Biol*. 2019;26(6):501-509. doi:10.1038/s41594-019-0236-8
58. Suzuki T, Terasaki M, Takemoto-Hori C, et al. Structural compensation for the deficit of rRNA with proteins in the mammalian mitochondrial ribosome. Systematic analysis of protein components of the large ribosomal subunit from mammalian mitochondria. *J Biol Chem*. 2001. doi:10.1074/jbc.M100432200
59. Thul PJ, Akesson L, Wiking M, et al. A subcellular map of the human proteome. *Science (80-)*. 2017. doi:10.1126/science.aal3321
60. Li H, Chen W, Zhou Y, et al. Identification of mRNA binding proteins that regulate the stability of LDL receptor mRNA through AU-rich elements. *J Lipid Res*. 2009. doi:10.1194/jlr.M800375-JLR200
61. Wilson GM, Vasa MZ, Deeley RG. Stabilization and cytoskeletal-association of LDL receptor mRNA are mediated by distinct domains in its 3' untranslated region. *J Lipid Res*. 1998.
62. Kim JH, Lee S-R, Li L-H, et al. High Cleavage Efficiency of a 2A Peptide Derived from Porcine Teschovirus-1 in Human Cell Lines, Zebrafish and Mice. Thiel V, ed. *PLoS One*. 2011;6(4):e18556. doi:10.1371/journal.pone.0018556
63. Collins R, Reith C, Emberson J, et al. Interpretation of the evidence for the efficacy and safety of statin therapy. *Lancet*. 2016;388(10059):2532-2561. doi:10.1016/S0140-6736(16)31357-5
64. Dinur M, Kilav R, Sela-Brown A, Jacquemin-Sablon H, Naveh-Many T. In vitro evidence that upstream of N-ras participates in the regulation of parathyroid hormone messenger ribonucleic acid stability. *Mol Endocrinol*. 2006. doi:10.1210/me.2005-0333
65. Boussadia O, Niepmann M, Créancier L, Prats A-C, Dautry F, Jacquemin-Sablon H. Unr Is Required In Vivo for Efficient Initiation of Translation from the Internal Ribosome Entry Sites of both Rhinovirus and Poliovirus. *J Virol*. 2003. doi:10.1128/jvi.77.6.3353-3359.2003
66. Dormoy-Raclet V, Markovits J, Jacquemin-Sablon A, Jacquemin-Sablon H. Regulation of Unr expression by 5′- and 3′-untranslated regions of its mRNA through modulation of stability and IRES mediated translation. *RNA Biol*. 2005. doi:10.4161/rna.2.3.2203
67. Duncan KE, Strein C, Hentze MW. The SXL-UNR Corepressor Complex Uses a PABP-Mediated Mechanism to Inhibit Ribosome Recruitment to msl-2 mRNA. *Mol Cell*. 2009. doi:10.1016/j.molcel.2009.09.042
68. Ray S, Anderson EC. Stimulation of translation by human Unr requires cold shock domains 2 and 4, and correlates with poly(A) binding protein interaction. *Sci Rep*. 2016. doi:10.1038/srep22461
69. Grosset C, Chen C-YA, Xu N, Sonenberg N, Jacquemin-Sablon H, Shyu A-B. A Mechanism for Translationally Coupled mRNA Turnover. *Cell*. 2000. doi:10.1016/s0092-8674(00)00102-1
70. Singh AB, Li H, Kan CFK, Dong B, Nicolls MR, Liu J. The critical role of mRNA destabilizing protein heterogeneous nuclear ribonucleoprotein D in 3′ untranslated region-mediated decay of low-density lipoprotein receptor mRNA in liver tissue. *Arterioscler Thromb Vasc Biol*. 2014. doi:10.1161/ATVBAHA.112.301131
71. Knouff C, Malloy S, Wilder J, Altenburg MK, Maeda N. Doubling Expression of the Low Density Lipoprotein Receptor by Truncation of the 3′-Untranslated Region Sequence

Ameliorates Type III Hyperlipoproteinemia in Mice Expressing the Human ApoE2 Isoform. *J Biol Chem*. 2001. doi:10.1074/jbc.M009423200

72. Bjune K, Wierød L, Naderi S. Triciribine increases LDLR expression and LDL uptake through stabilization of LDLR mRNA. *Sci Rep*. 2018. doi:10.1038/s41598-018-34237-6
73. Kong W, Wei J, Abidi P, et al. Berberine is a novel cholesterol-lowering drug working through a unique mechanism distinct from statins. *Nat Med*. 2004. doi:10.1038/nm1135
74. Moore KS, Yagci N, Van Alphen F, et al. Csde1 binds transcripts involved in protein homeostasis and controls their expression in an erythroid cell line. *Sci Rep*. 2018. doi:10.1038/s41598-018-20518-7
75. Ju Lee H, Bartsch D, Xiao C, et al. A post-transcriptional program coordinated by CSDE1 prevents intrinsic neural differentiation of human embryonic stem cells. *Nat Commun*. 2017. doi:10.1038/s41467-017-01744-5
76. Dormoy-Raclet V, Markovits J, Malato Y, et al. Unr, a cytoplasmic RNA-binding protein with cold-shock domains, is involved in control of apoptosis in ES and HuH7 cells. *Oncogene*. 2007. doi:10.1038/sj.onc.1210068
77. Ray KK, Wright RS, Kallend D, et al. Two phase 3 trials of inclisiran in patients with elevated LDL cholesterol. *N Engl J Med*. 2020. doi:10.1056/NEJMoa1912387
78. McClure KF, Piotrowski DW, Petersen D, et al. Liver-Targeted Small-Molecule Inhibitors of Proprotein Convertase Subtilisin/Kexin Type 9 Synthesis. *Angew Chemie Int Ed*. 2017;56(51):16218-16222. doi:10.1002/anie.201708744
79. Gibson DG, Young L, Chuang R-Y, Venter JC, Hutchison CA, Smith HO. Enzymatic assembly of DNA molecules up to several hundred kilobases. *Nat Methods*. 2009;6(5):343-345. doi:10.1038/nmeth.1318
80. Chorba JS, Galvan AM, Shokat KM. Stepwise processing analyses of the single-turnover PCSK9 protease reveal its substrate sequence specificity and link clinical genotype to lipid phenotype. *J Biol Chem*. 2018;293(6):1875-1886. doi:10.1074/jbc.RA117.000754
81. Adamson B, Norman TM, Jost M, et al. A Multiplexed Single-Cell CRISPR Screening Platform Enables Systematic Dissection of the Unfolded Protein Response. *Cell*. 2016;167(7):1867-1882.e21. doi:10.1016/j.cell.2016.11.048
82. Mi H, Muruganujan A, Huang X, et al. Protocol Update for large-scale genome and gene function analysis with the PANTHER classification system (v.14.0). *Nat Protoc*. 2019. doi:10.1038/s41596-019-0128-8
83. Bateman A. UniProt: A worldwide hub of protein knowledge. *Nucleic Acids Res*. 2019. doi:10.1093/nar/gky1049
84. Sudlow C, Gallacher J, Allen N, et al. UK Biobank: An Open Access Resource for Identifying the Causes of a Wide Range of Complex Diseases of Middle and Old Age. *PLoS Med*. 2015. doi:10.1371/journal.pmed.1001779
85. Loh PR, Tucker G, Bulik-Sullivan BK, et al. Efficient Bayesian mixed-model analysis increases association power in large cohorts. *Nat Genet*. 2015. doi:10.1038/ng.3190
86. Baker JM, Boyce FM. High-throughput functional screening using a homemade dual-glow luciferase assay. *J Vis Exp*. 2014. doi:10.3791/50282
87. Higgins JPT GS (editors). Cochrane Handbook for Systematic Reviews of Interventions Version 5.1.0 . The Cochrane Collaboration .

Figures and Figure Legends

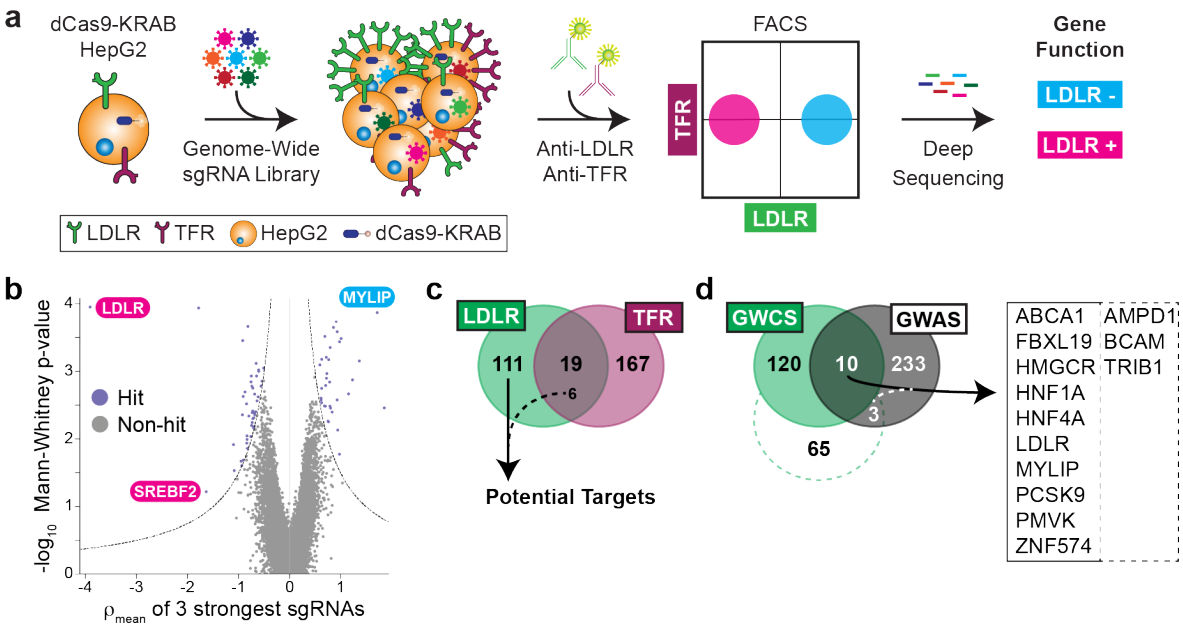

Figure 1: Genome-Wide CRISPR Interference Screen. *a)* Overall schematic of selection. See text for details. *b)* Volcano plot showing the statistical significance (Mann-Whitney test) of the guides recovered for each gene against the mean ρ phenotype of the three guides with the strongest effect. ρ is defined as the $\log_2$-fold enrichment for high LDLR expressing cells to the low LDLR expressing cells. Guides targeting known regulators of the LDLR are noted. *c)* Venn diagram showing the overlap between parallel LDLR and TFR screens. 6 guides common to both had opposing expression phenotypes in the respective screens, and were included as specific hits. *d)* Venn diagram of hits between the LDLR screen (GWCS) and putative genes correlated with serum LDL from GWAS. The dotted line indicates a relaxed threshold for hit selection from LDLR screen, with only an additional 3 genes in the overlap. Overlap genes shown at right.

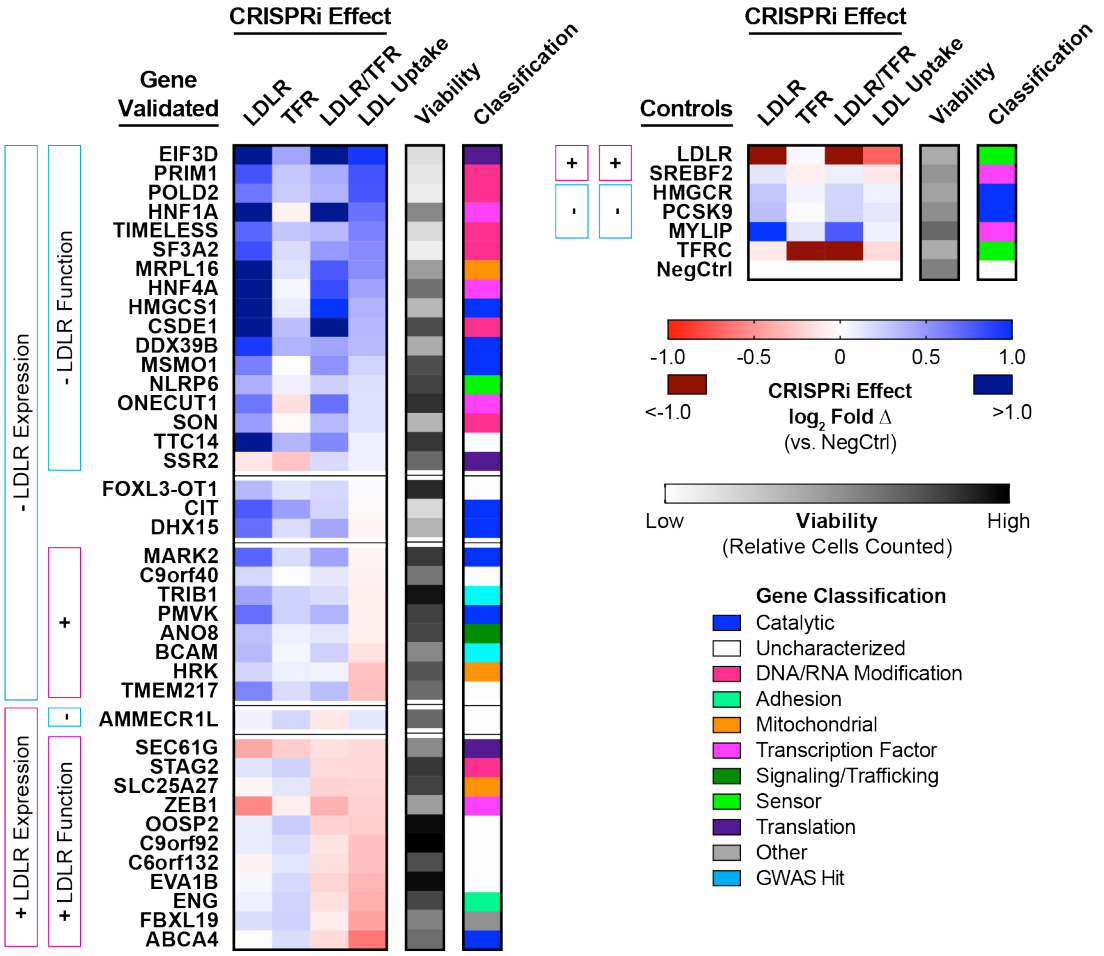

Figure 2: Validation of LDLR CRISPRi Hits. Heatmap showing receptor expression (LDLR, TFR, and LDLR/TFR ratio) and receptor function (LDL uptake) for dCas9-KRAB HepG2 cells transduced with sgRNA targeting the indicated gene, analyzed by flow cytometry. Hits are grouped according to directional effect on LDLR expression, and then within groups, by effect on LDL uptake (with uptake from *FOXL3-OT1*, *CIT*, and *DHX15* sgRNAs not significantly different from negative control sgRNA). Readouts show $\log_2$ fold change compared to transduction with negative control sgRNA, and represent the weighted average of the effects from both sgRNAs targeting each gene. Viability indicates the relative number of cells evaluated in the experiments. Genes classified as per evaluation in Extended Data Fig. 3. Note that LDLR/TFR is a separately ascertained value from individual cells, and not a derived parameter from aggregate data. Only the hits for which two separate sgRNAs independently validated for receptor expression are shown, defined as $p < 0.05$ via Holm-Sidak corrected T-test. Data represent summary information from 3 to 4 independent experiments.

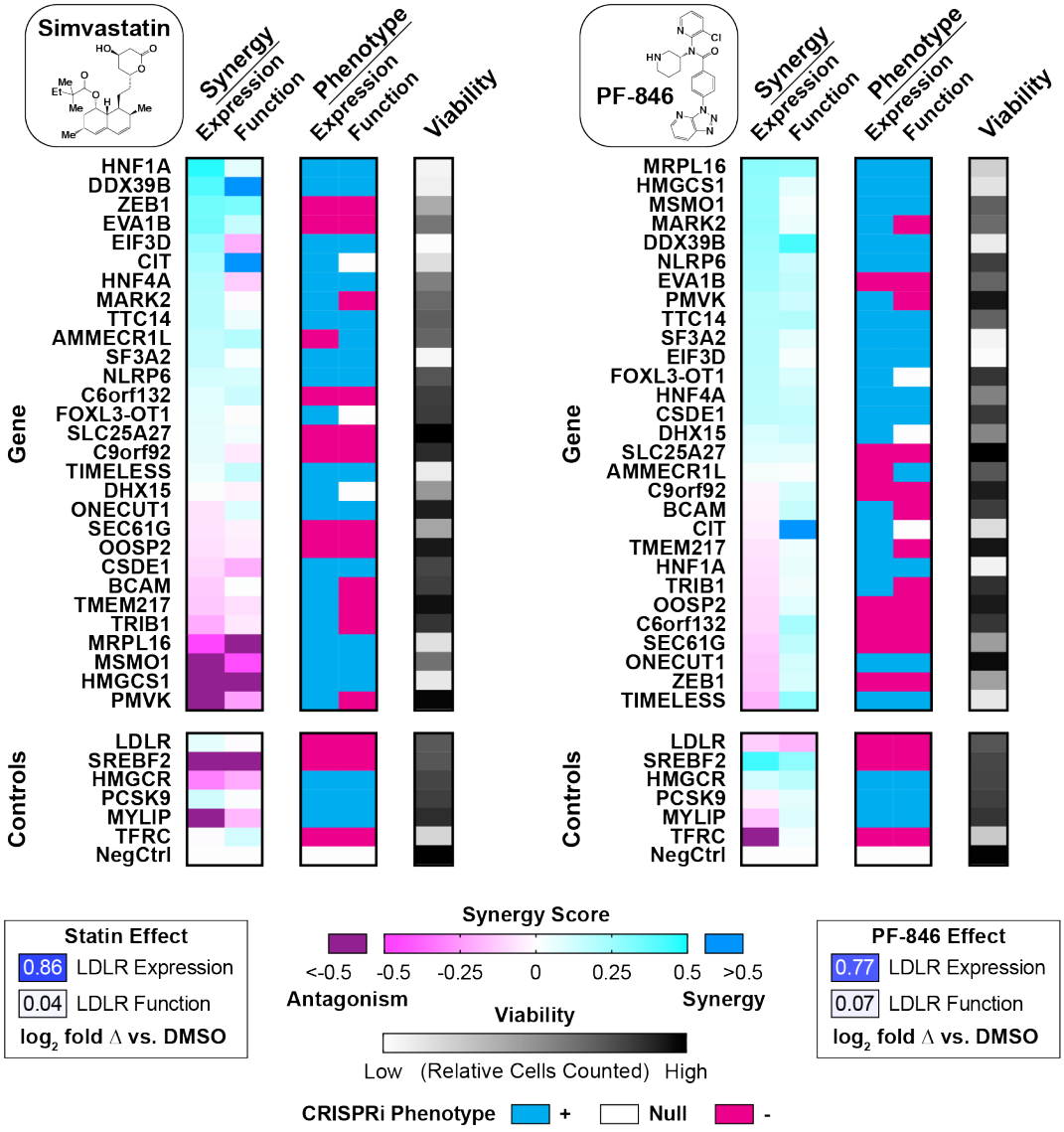

Figure 3: CRISPRi Knockdown Synergy with Statin and PF-846. Heatmap showing synergy score with statin (left) or PF-846 (right) for knockdowns of indicated genes with a single validated sgRNA for separate LDLR expression and function experiments. LDLR/TFR ratio and LDL uptake from flow cytometry experiments represent expression and function, respectively. Baseline effects of the compound on cells transduced with negative control sgRNA are shown in legend ($p < 0.001$ by Holm-Sidak corrected T-test). CRISPRi phenotype from the validation experiments shown for comparison. As in Figure 2, viability indicates the relative number of cells evaluated in the experiments. Data represent summary information from 4 independent experiments.

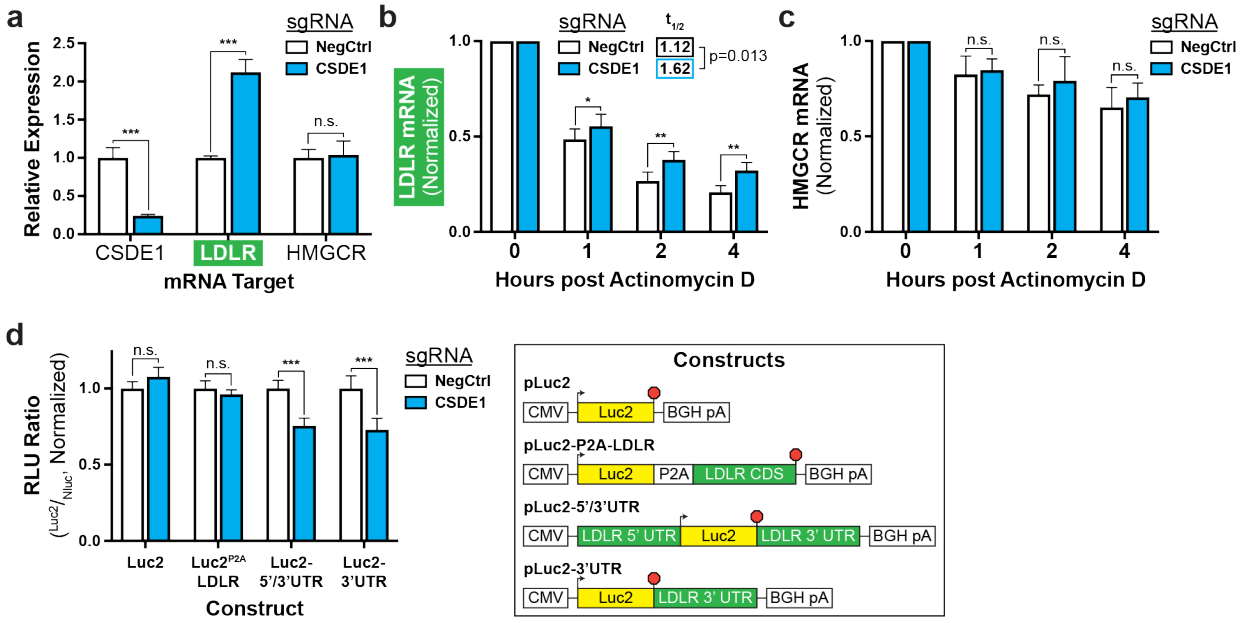

Figure 4: CSDE1 Mediates LDLR mRNA Decay. *a)* Relative expression, by qPCR, of *LDLR*, *HMGCR*, and *CSDE1* in engineered dCas9-KRAB HepG2 cells transduced with indicated sgRNAs and subsequently sterol-depleted. *b)* Relative expression, by qPCR, of LDLR mRNA transcripts in dCas9-KRAB HepG2 cells with indicated sgRNA after arrest of transcription with actinomycin D. Data are normalized to results at T=0 within the sgRNA evaluated, so as to illustrate the change in time. $t_{1/2}$ shown indicates the best fit data to a one-stage exponential decay equation. *c)* Relative expression of HMGCR transcripts in same experiment as *b*. *d)* Relative ratiometric luciferase activity for transient transfections of indicated luciferase reporter constructs, using dCas9-KRAB HepG2 cells harboring sgRNA targeting *CSDE1* vs. negative control sgRNA. Schematics of constructs shown, illustrating CMV promoter, start site (arrowhead), stop codon (red octagon), and BGH polyadenylation signal. Transfections performed with 6 replicates per experiment, with individual wells normalized to a secreted luciferase control (pSS-NLuc). For all panels, error bars indicate 95% confidence intervals. Data represent summary information from 3-4 independent experiments. * = $p < 0.05$, ** = $p < 0.01$, and *** = $p < 0.001$ (Holm-Sidak corrected T-test).

Supplemental and Extended Data

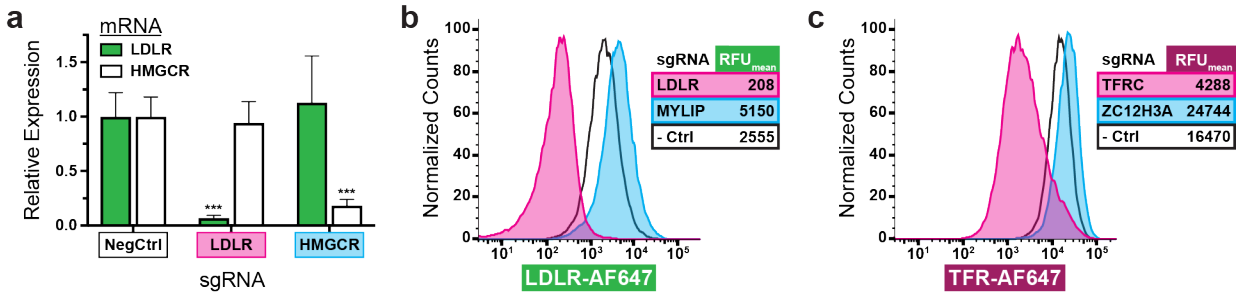

Extended Data Figure 1: Validation of dCas9-KRAB-HepG2 Cells. *a)* Relative expression, by qPCR, of *LDLR* and *HMGCR* in engineered dCas9-KRAB HepG2 cells transduced with sgRNAs targeting the indicated genes. *B2M* used as qPCR control. Error bars indicate 95% CI. *** = p < 0.001 by Holm-Sidak corrected T-test, comparing to negative control sgRNA of the same target. *b)* Flow cytometry analysis, by surface labelling with anti-LDLR-AF647, of dCas9-KRAB HepG2 cells transduced with sgRNAs targeting the indicated genes. *MYLIP* (IDOL) is an E3 ligase which ubiquitinates the LDLR, leading to lysosomal degradation[24]. *c)* Flow cytometry analysis as in *b*, but transduced with indicated sgRNAs and labelled with anti-TFR-AF647. *ZC3H12A* (REG1) is an endoribonuclease that accelerates the degradation of TFR mRNA[25].

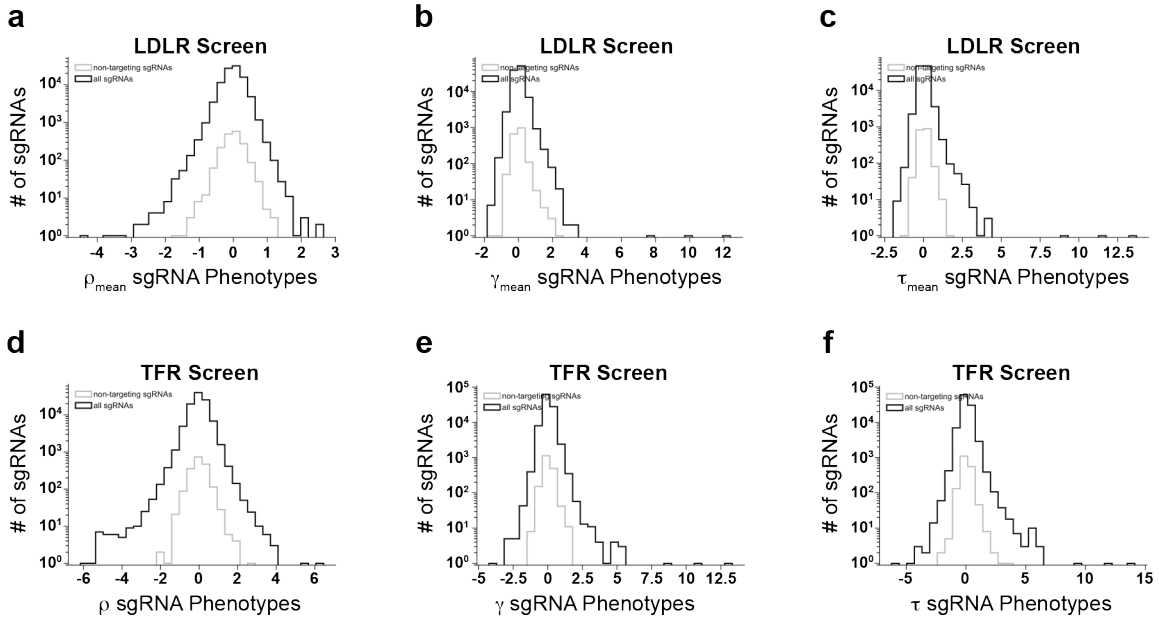

Extended Data Figure 2: Recovered sgRNAs from Screening Phenotypes. Distribution of number of guide RNAs recovered by phenotype in both LDLR (*a-c*) and TFR (*d-f*) screens. ρ (*a,d*) indicates $\log_2$ fold enrichment for sgRNA in high receptor expressing cells compared to low receptor expressing cells. γ (*b,e*) indicates $\log_2$ enrichment for sgRNA in low receptor expressing cells compared to unsorted population. τ (*c,f*) indicates $\log_2$ enrichment for sgRNA in high receptor expressing cells compared to unsorted population. Mean results are reported for the 3 replicates of the LDLR screen (*a-c*).

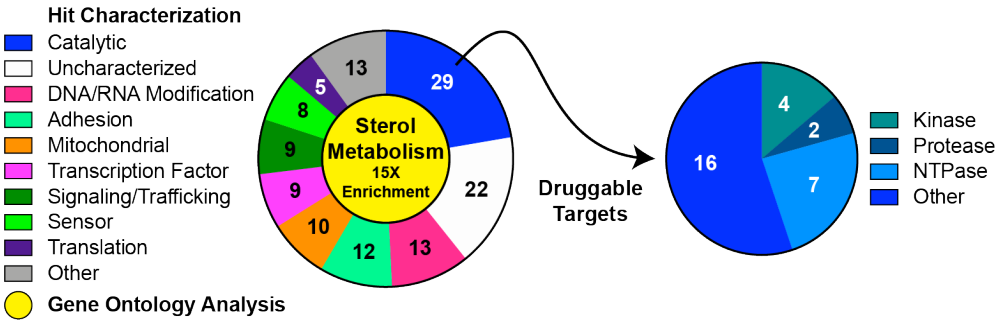

Extended Data Figure 3: Gene Ontology and Localization Analysis. Characterization of hits from the LDLR screen based on gene ontology (GO) and localization, along with results from GO enrichment analysis (yellow center). Note that multiple genes fall into more than one category.

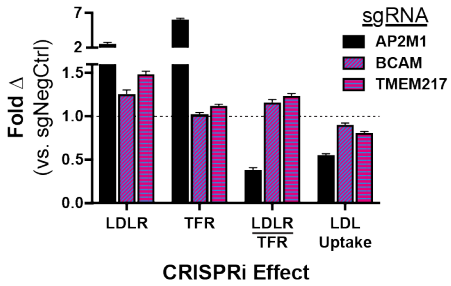

Extended Data Figure 4: Selective LDLR Effect on Transmembrane Proteins. Flow cytometric readout of receptor expression and LDLR function assays, using CRISPRi knockdowns against genes thought to be involved in endocytosis. Data, which represents 3 to 4 independent experiments, are normalized to readout of negative control sgRNA within each experiment. Error bars represent 95% confidence intervals. Note the discontinuous Y axis.

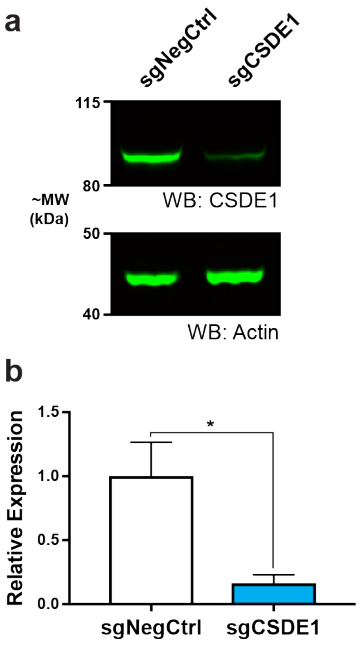

Extended Data Figure 5: CSDE1 Knockdown at Protein Level. *a*) Representative immunoblots of lysates of dCas9-KRAB HepG2 cells harboring indicated guide RNA. CSDE1 shown above, and β-actin (loading control) shown below. *b*) Quantification of relative expression of CSDE1 (normalized to loading control) shown in immunoblot in *a*. Data includes 3 independent experiments. * indicates $p < 0.05$ by Welch's T-test.

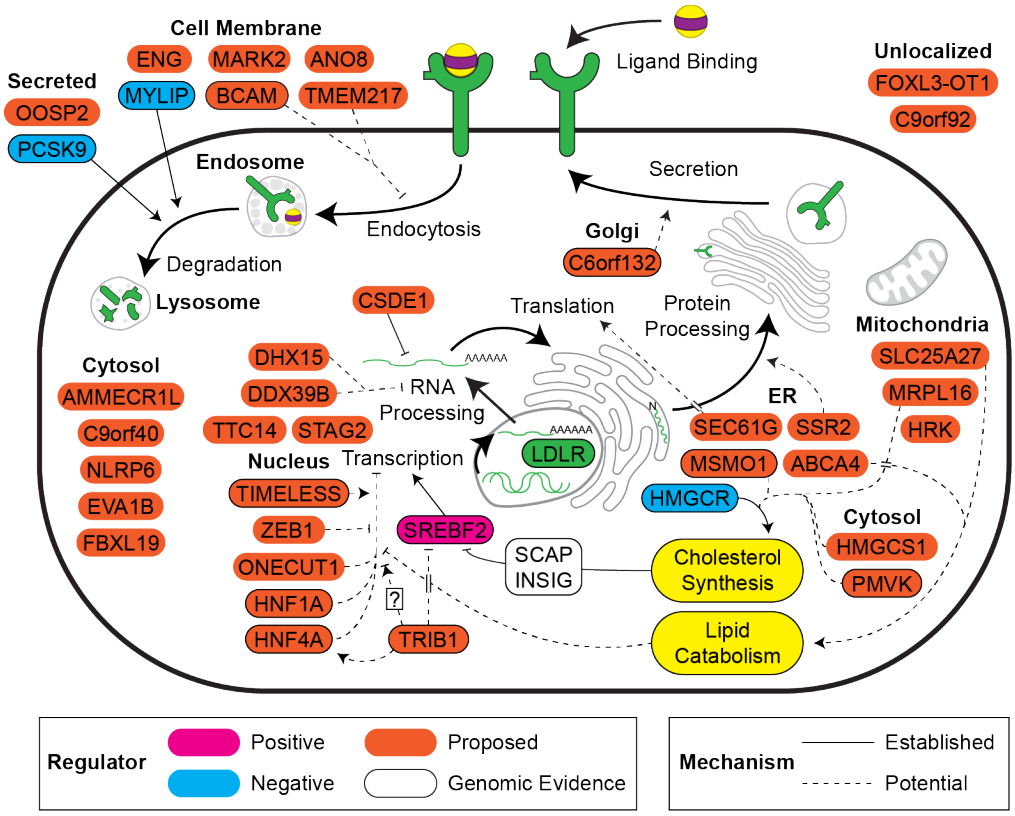

Extended Data Figure 6: An Exploratory Map of Potential LDLR Regulatory Targets. Genes identified and validated in the screen are mapped by cellular localization and possible mechanisms of effect. Known downregulators are shown in cyan, and known upregulators shown in magenta. Validated hits with observed effects on cell proliferation or viability are excluded.

Extended Data Tables

LDLR Hits	TFR Hits	LDLR Specific Hits	LDLR Specific Hits (NCBI Name)
ABCA1	A4GNT	ABCA1	ABCA1
ABCA4	ABCC10	ABCA4	ABCA4
ACAN	ACO1	ACAN	ACAN
ACO1	ACSL5	ALKBH5	ALKBH5
ALKBH5	ANKRD33	AMMECR1L	AMMECR1L
AMMECR1L	AP2A2	ANO8	ANO8
ANO8	AP2M1	BCAR1	BCAR1
BCAR1	AP2S1	C12orf45	C12orf45
C12orf45	ARSE	C14orf79	CLBA1
C14orf79	ATP6AP1	C1orf210	C1orf210
C1orf210	ATP6V1B2	C5orf34	C5orf34
C5orf34	BRS3	C6orf132	C6orf132
C6orf132	C10orf128	C9orf40	C9orf40
C9orf40	C14orf166	C9orf92	C9orf92
C9orf92	C3orf17	CD164L2	CD164L2
CD164L2	C3orf72	CD276	CD276
CD276	CCDC105	CD96	CD96
CD96	CDH13	CIT	CIT
CIT	CENPE	CSDE1	CSDE1
CLTC	CERS3	CXCR2	CXCR2
CSDE1	CHTF18	CXXC11	FBXL19
CXCR2	CKMT1A	CYB5R3	CYB5R3
CXXC11	CLTC	DDX39B	DDX39B
CYB5R3	COL20A1	DESI1	DESI1
DDX39B	COPZ1	DHX15	DHX15
DESI1	CYB5R3	DUOX1	DUOX1
DHX15	DDX23	EIF3D	EIF3D
DUOX1	DNM2	ENG	ENG
EIF3D	EIF2B3	ENTPD1	ENTPD1
ENG	EIF2S1	ESRRG	ESRRG
ENTPD1	EIF3G	EVA1B	EVA1B
ESRRG	ELK1	FAM126A	FAM126A
EVA1B	ELOVL5	FAM178B	FAM178B
FAM126A	ENO4	FAM57A	TLCD3A
FAM178B	EPGN	FBXW11	FBXW11
FAM57A	F8A2	FDPS	FDPS

FBXW11	F8A3	GXYLT1	GXYLT1
FDPS	FBL	HMGCR	HMGCR
GXYLT1	FBXL5	HMGCS1	HMGCS1
HMGCR	FIP1L1	HNF1A	HNF1A
HMGCS1	FLYWCH2	HNF4A	HNF4A
HNF1A	GAB4	HPGDS	HPGDS
HNF4A	GNA12	HRK	HRK
HPGDS	HARS	ICAM4	ICAM4
HRK	HEATR1	INTS8	INTS8
ICAM4	HGC6.3	ITGA11	ITGA11
INTS8	HNF4A	ITGA7	ITGA7
ITGA11	IFNAR2	ITGAV	ITGAV
ITGA7	IGFL2	LDLR	LDLR
ITGAV	INCENP	LGALS14	LGALS14
KIAA0895	IPO13	LOC100288524	FOXL3-OT1
LDLR	IRS1	LOC729159	NPAP1L
LGALS14	ITGA6	LYZ	LYZ
LOC100288524	KANSL2	MARK2	MARK2
LOC729159	KHDC1L	MATN1	MATN1
LYZ	KIAA0895	MFHAS1	MFHAS1
MARK2	KRT18	MRAP2	MRAP2
MATN1	LCN10	MRPL16	MRPL16
MBOAT1	LOC100129216	MRPL22	MRPL22
MFHAS1	LOC100130705	MSMO1	MSMO1
MRAP2	LOC158434	MYLIP	MYLIP
MRPL16	LOC200726	NCR2	NCR2
MRPL22	LST1	NDUFB5	NDUFB5
MRPL35	LY6K	NDUFS8	NDUFS8
MSMO1	LYPD3	NINJ1	NINJ1
MYLIP	MAK16	NLRP6	NLRP6
NCR2	MBOAT1	ONECUT1	ONECUT1
NDUFA8	MCM10	OR52A1	OR52A1
NDUFB2	MGAT3	PCDH7	PCDH7
NDUFB5	MPZL1	PCDHB4	PCDHB4
NDUFS8	MRFAP1	PCSK9	PCSK9
NINJ1	MRPL35	PHGR1	PHGR1
NLRP6	MRPS12	PIANP	PIANP
NPY4R	MSS51	PID1	PID1
ONECUT1	MYLK4	PLAC1L	OOSP2

OR52A1	NDUFA8	PMVK	PMVK
PCDH7	NDUFB2	POLD2	POLD2
PCDHB4	NDUFB6	POLD3	POLD3
PCSK9	NPPA	PRIM1	PRIM1
PHGR1	NPY4R	PROL1	OPRPN
PIANP	NR5A1	PTGDR2	PTGDR2
PID1	NSRP1	RARRES3	PLAAT4
PLAC1L	NUDCD3	REPS1	REPS1
PMVK	OR11H4	RNF151	RNF151
POLD2	OR4D10	RSG1	CPLANE2
POLD3	OTUD3	SCUBE1	SCUBE1
PRIM1	PCDHA1	SEC61G	SEC61G
PROL1	PCDHGA9	SERPINA9	SERPINA9
PTGDR2	PCSK9	SF3A2	SF3A2
RARRES3	PHLDB1	SLC25A27	SLC25A27
REPS1	PKDREJ	SLC2A7	SLC2A7
RNF151	PLD1	SLC6A19	SLC6A19
RPA2	PLEKHG5	SLURP1	SLURP1
RPS18	PMP2	SMURF1	SMURF1
RSG1	POLR2H	SON	SON
SCUBE1	POP1	SREBF2	SREBF2
SEC61A1	PPIE	SSR2	SSR2
SEC61G	PPP1R8	SSUH2	SSUH2
SERPINA9	PRPF3	ST6GALNAC4	ST6GALNAC4
SF3A2	PRPH2	STAC	STAC
SLC25A27	PRRC2A	STAG2	STAG2
SLC2A7	PSMA1	TIMELESS	TIMELESS
SLC6A19	PSMA3	TMEM217	TMEM217
SLURP1	PSMA4	TMEM86A	TMEM86A
SMURF1	PSMA5	TPRG1	TPRG1
SON	PSMB2	TRMT10C	TRMT10C
SREBF2	PSMB6	TRPM1	TRPM1
SSR2	PSMC4	TRPM7	TRPM7
SSUH2	PSMD13	TTC14	TTC14
ST6GALNAC4	PSMD4	TXNDC8	TXNDC8
STAC	PSMD6	WDR5	WDR5
STAG2	PSMD7	WDR75	WDR75
TFRC	PTPN22	ZBED6CL	ZBED6CL
TIMELESS	PWP2	ZBTB42	ZBTB42

TMEM217	PWWP2A	ZC3H12A	ZC3H12A
TMEM86A	QRICH2	ZEB1	ZEB1
TPRG1	RAB5C	ZNF595	ZNF595
TRMT10C	RBM8A		
TRPM1	RPA2		
TRPM7	RPL15		
TTC14	RPL17		
TXNDC8	RPL18		
WDR5	RPL23		
WDR75	RPL24		
ZBED6CL	RPL26		
ZBTB42	RPL27		
ZC3H12A	RPL27A		
ZEB1	RPL31		
ZNF574	RPL34		
ZNF595	RPL36		
	RPL37A		
	RPL38		
	RPL4		
	RPL6		
	RPL7A		
	RPL8		
	RPL9		
	RPP25L		
	RPS13		
	RPS14		
	RPS18		
	RPS20		
	RPS23		
	RPS27A		
	RPS29		
	RPS8		
	RPSA		
	SEC61A1		
	SELE		
	SERPIND1		
	SF3A1		
	SF3A2		
	SF3B4		

	SH2D3A		
	SHOC2		
	SIGIRR		
	SIRT2		
	SLC12A9		
	SLC2A7		
	SLC44A3		
	SLC45A1		
	SMU1		
	SNRPF		
	SRL		
	SUSD1		
	TAS2R7		
	TCP11		
	TFRC		
	TGM5		
	THOC7		
	TMEM229A		
	TMEM40		
	TMIGD2		
	TPBG		
	TRAPPC13		
	TRAPPC6A		
	TTC12		
	TUBB		
	TXNDC8		
	VCP		
	VPS16		
	VPS29		
	VPS41		
	VPS9D1		
	VWA2		
	ZNF574		

Extended Table 1: CRISPRi Screening Hits.

Metric	Value
Age (y)	56.9 (7.9)
Sex	179,963 (46.1%)
European ancestry	376,358 (96.4%)
Cholesterol (mg/dl)	
Total	221.1 (44.3)
HDL	56.1 (14.8)
LDL	138.1 (33.7)
Triglycerides (mg/dl)	132.6 [93.6-191.5]
Statin Rx	64,004 (16.4%)
BMI (kg/m^2)	27.4 (4.8)
Systolic blood pressure (mmHg)	140.2 (19.7)
Diastolic blood pressure (mmHg)	82.3 (10.7)
Current smoker	39,736 (10.2%)
Diabetes mellitus type 2	25,349 (6.5%)
Coronary artery disease	18,204 (4.8%)

Extended Data Table 2: Baseline Characteristics of UK Biobank Participants in Genomic Association Analyses. Continuous values are presented as mean (standard deviation) except for triglycerides which is given as median (Q1-Q3) due to the skewness of the triglyceride distribution. Categorical data are presented as count (percentage). BMI = body-mass index; HDL = high-density lipoprotein; LDL = low-density lipoprotein.

GENE	Variant rsID	BETA	P_BOLT_LMM	Consequence	IMPACT
HNF4A	rs1800961	0.0564144	0	missense_variant	MODERATE
BCAM	rs28399659	-0.0174111	7.70E-29	missense_variant	MODERATE
BCAM	rs200398713	-0.0803165	1.80E-28	splice_region_variant,intron_variant	LOW
BCAM	rs199922856	-0.342179	6.20E-28	missense_variant	MODERATE
BCAM	rs28399654	0.220592	6.10E-10	missense_variant	MODERATE
BCAM	rs3810141	0.020077	5.50E-07	stop_gained	HIGH
TIMELESS	rs2291738	0.00388393	0.00014	splice_region_variant,intron_variant	LOW
BCAM	rs149302547	-0.147327	0.005	missense_variant	MODERATE
BCAM	rs1135062	-0.0213642	0.0074	missense_variant	MODERATE
C6orf132	rs55772414	0.0116856	0.013	missense_variant	MODERATE
MSMO1	rs142496142	0.0432195	0.015	missense_variant	MODERATE

Extended Data Table 3: Association of Nonsynonymous Variants in CRISPRi Screen Hits with Serum LDL-C in the UK Biobank. BETA indicates the linear regression standardized effect size, and P_BOLT_LMM indicates the linear mixed model p value using BOLT-LMM[85].